

# Measurement of the Stratum Radiatum/Lacunosum-Moleculare (SRLM)

Steffen Oeltze<sup>1</sup>, Hartmut Schütze<sup>2</sup>, Anne Maaß<sup>2</sup>, Emrah Düzel<sup>2,3,4</sup>,  
Bernhard Preim<sup>1</sup>

<sup>1</sup>Department of Simulation and Graphics, University of Magdeburg

<sup>2</sup>Institute of Cognitive Neurology and Dementia Research, University of Magdeburg

<sup>3</sup>German Centre for Neurodegenerative Diseases (DZNE), Standort Magdeburg

<sup>4</sup>Institute of Cognitive Neuroscience, University College London, UK

stoeltze@isg.cs.uni-magdeburg.de

**Abstract.** Alzheimer disease (AD) at an early stage is characterized by a synaptic loss and atrophy in the apical layer of the CA1 part of the hippocampus, the stratum radiatum and stratum lacunosum-moleculare (SRLM). It was shown in vivo that patients with mild AD exhibit a reduced thickness of the SRLM.

We propose a new approach to measure SRLM thickness in coronal brain sections. It is based on the interpolated contour of the manually segmented SRLM and its medial axis. We automatically compute the axis by combining Voronoi diagrams and methods from graph analysis. While existing measurement approaches require a manual segmentation of the SRLM and a repeated local estimate of its center, we obviate the latter. We evaluate our approach based on coronal  $T2^*$ -weighted 7-Tesla MR images of 27 subjects.

## 1 Introduction

At an early stage, Alzheimer disease (AD) is characterized by episodic memory dysfunction. The hippocampus – a brain structure existing in both hemispheres and being part of the limbic system – plays a crucial role in consolidating episodic memory [1]. Postmortem studies found that synaptic loss and atrophy in the apical layer of the CA1 part of the hippocampus, the stratum radiatum and stratum lacunosum-moleculare (SRLM, Fig. 1(a)), coincide with earliest cognitive symptoms [2]. Kerchner et al. [3] showed that patients with mild AD exhibit a reduced SRLM thickness. Their analysis was based on coronal  $T2^*$ -weighted images from ultra-high field 7-Tesla (7-T) MRI. Only ultra-high field imaging provides an in-plane resolution ( $< \approx 0.5$  mm) high enough to identify hippocampal subfields (Fig. 1(b)). Since normal SRLM thickness is about 1 mm, its width covers only a few pixels. Within each transection of the hippocampus, the SRLM is heavily quantized and borders to adjacent structures form a step-wise pattern. Since the CA1 apical neuropil is affected in early stages of AD, a correct measurement of SRLM thickness could serve as an objective imaging biomarker for AD pathology and moreover, contribute to judging the (e.g. protective) effects of physical or cognitive training in early AD patients as well as healthy older people.

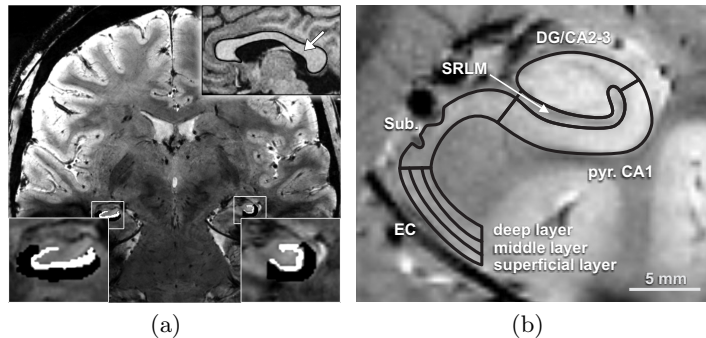


**Fig. 1.** (a) Coronal  $T2^*$ -weighted Magnetic Resonance image with overlaid ROIs of the stratum radiatum and stratum lacunosum-moleculare (SRLM, white) and pyramidal CA1 (black). The upper inset shows the corpus callosum (arrow). Its shape is similar to SRLM shape. (b) Schematic of the subfields in the hippocampal body.

Two approaches to measuring SRLM thickness have been published. A manual approach was presented by Kerchner et al. [3]. For each hemisphere in two consecutive slices, the user draws three lines extending over the local width of the SRLM. The approach is subjective, it is restricted to a subset of the slices that show the SRLM, and it poorly acknowledges the variance in thickness along the SRLM. Recently, Kerchner et al. [4] proposed a semi-automatic measurement. The user first draws in the medial axis of the SRLM in all slices. Orthogonal signal intensity profiles are then determined at equidistantly sampled points along a spline that is fit to the user-defined line. A single thickness value is computed per slice based on the average signal intensity change from the medial axis of the SRLM to the surrounding subfields. The approach is less subjective but sensitive to the user's definition of the medial axis. The definition requires a mental segmentation of the SRLM and a concurrent, repeated local estimate of its center. The latter is particularly tedious in regions of very small SRLM thickness (1-2 pixels). Furthermore, the measured local thickness depends on the signal intensity distribution of the surrounding subfields. SRLM sites being equally thick may result in different measurement values. This effect is mitigated by averaging the local intensity profiles but hampers a real local analysis.

The shape of the SRLM in coronal slices is similar to the shape of the *corpus callosum* (cc) in mid-sagittal slices (Fig. 1(a), cc in upper inset). An overview of approaches to measuring callosal thickness is part of [5]. Most approaches rely on the medial axis of the cc and determine thickness orthogonal to it. We propose a related SRLM measurement approach which is based on the interpolated contour of the manually segmented SRLM and the medial axis of this contour, i.e., of the SRLM. In contrast to [4], we automatically compute the axis. The contour increases the range of possible measurements, e.g., by area or curvature. Another advantage is the coherent local computation of SRLM thickness independent of the signal intensities of surrounding structures. We evaluate our approach based on two studies comprising  $T2^*$ -weighted 7-T MR images of 27 subjects.

## 2 Materials and Methods

The focus of this section is on the measurement of the SRLM. Before, we describe our study data and briefly our SRLM segmentation.

### 2.1 Study Data and SRLM Segmentation

The data were collected in an ultra-high field 7-T MRI study at the Institute of Cognitive Neurology and Dementia Research of the University of Magdeburg, Germany. The study combined a visual learning paradigm with high resolution functional measurements and very high resolution structural images for 14 subjects. A pre-study with 13 subjects was conducted. For both studies, healthy young people were recruited (age  $25 \pm 2$ , 14 male). MRI data were acquired using a 7-T MRI system (Siemens, Erlangen, Germany) with a 32-channel head coil. The high resolution partial structural volume was acquired (T2\*-weighted imaging,  $TE = 18.5$  ms,  $TR = 680$  ms, in-plane resolution  $0.33$  mm  $\times$   $0.33$  mm, slice thickness  $1.5$  mm + 25% gap, 45 slices, FOV  $212$  mm  $\times$   $179$  mm, matrix  $640 \times 540$ ), with a slice alignment orthogonal to the hippocampal main axis. The pre-study was conducted with the same sequence and similar parameters.

The segmentation of hippocampal subfields was performed for each hemisphere using MRIcron (Chris Rorden, Version 4, April 2011). First, subfields in the hippocampal body were traced according to [6]. Next, the parahippocampal regions were delineated. Then, the hippocampal head was segmented into subregions according to [7]. The hippocampal tail was not delineated. Overall, the hippocampus was segmented into subiculum (Sub), CA1-stratum pyramidale (pyr. CA1), CA1-stratum radiatum/stratum lacunosum-moleculare (SRLM, Fig. 1(b)) and the remaining portion comprising CA2, CA3, and DG (DG/CA2-3). Only the SRLM part in the hippocampal body is used in the thickness evaluation.

### 2.2 SRLM Measurement

Our measurement of the SRLM is based on its medial axis. A good survey of medial axis computation algorithms is part of [8]. The pixel-based medial axis generated by topological thinning or distance transform algorithms is too coarse since the width of the SRLM in some regions covers only 1-2 pixels. Surface sampling methods allow for a more fine-grained determination but require a representation of the objects boundary by a dense cloud of sample points. Our measurement algorithm starts by computing this point cloud.

Given the binary mask of the SRLM resulting from segmentation, we process this mask slice-by-slice (Fig. 2(a)). A 3D measurement is not feasible due to the considerable slice thickness ( $1.5$  mm + 25% gap). We start by computing a smooth contour of the quantized binary mask. A marching squares algorithm with linear interpolation provides an initial sharp-edged contour. The contour is enhanced via B-spline interpolation followed by a Laplacian smoothing with displacement adjustment to avoid shrinkage [9]. The smoothing parameters have been determined empirically: 10 smoothing passes with a factor of 0.1 and a window of 3

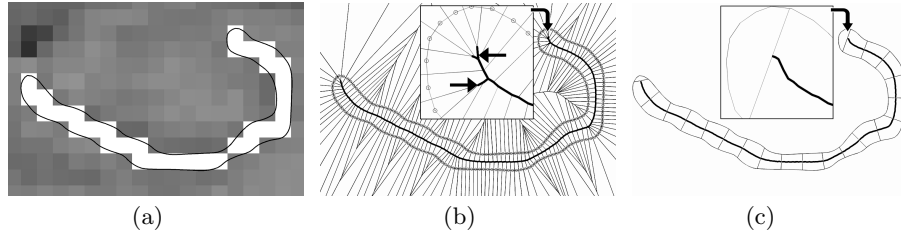


**Fig. 2.** Measurement approach. (a) Computation of the contour (black) of the SRLM mask (white). (b) Voronoi diagram (net-like structure) of the contour points (circles). The medial axis (thick polyline) is part of the diagram. The inset shows erroneous side branches. (c) Ideal medial axis and thickness measurements (thin, orthogonal lines).

points. The final contour is resampled equidistantly with a sample point density that fulfills the requirements for an accurate medial axis computation [10].

The medial axis is derived from the Voronoi diagram of the sample points [10] (Fig. 2(b)). A Voronoi diagram divides the space into regions such that each seed (contour sample point) is contained in a separate region which comprises all points that are closer to this seed than to any other. The edges of the Voronoi diagram, which are completely contained within the SRLM contour, constitute its medial axis. They are determined based on point-in-polygon tests. The Voronoi approach is sensitive to noise in the contour. Slight deviations from a perfectly smooth curve cause short side branches originating from the medial axis (inset in Fig. 2(b)). Hence, pruning is often carried out as a post-processing step [10].

We suggest an inverse strategy that separates the ideal medial axis  $MA_{ideal}$  from the noisy one  $MA_{noisy}$  (Fig. 2(c)). Due to the normally non-branching, tubular shape of the SRLM within a coronal slice,  $MA_{ideal}$  is a simple polyline extending from one end to the other. Its separation is based on the observation that  $MA_{ideal}$  corresponds to the longest of the shortest paths between any pair of terminal vertices of  $MA_{noisy}$ . We treat  $MA_{noisy}$  as an undirected, unweighted, acyclic graph. Each of the  $n$  vertices is a node and an edge exists between two nodes if they are connected by a line segment in  $MA_{noisy}$ . We describe the graph by its  $n \times n$  symmetric adjacency matrix  $A$ , whose entries equal 1 if the two corresponding nodes are connected by an edge and 0 otherwise. Terminal vertices of  $MA_{noisy}$  are characterized by a single 1 in their corresponding row or column of  $A$ . For each pair of terminal vertices, we find the shortest in-between path, i.e., along  $MA_{noisy}$ , by Breadth-First Search on  $A$ . The longest of these shortest paths represents  $MA_{ideal}$ .

To measure SRLM thickness, we equidistantly resample  $MA_{ideal}$  according to a user-defined number of thickness measurements (Fig. 2(c)). At each sample point, we erect an orthogonal line. Its intersections with the lower and upper part of the SRLM's contour delimit the local thickness. If a line intersects the contour more than twice, the two intersections which are on either side of the line and closest to  $MA_{ideal}$  are chosen. The Euclidean distance between the intersection points corresponds to the local thickness of the SRLM.

### 3 Results

We have applied our measurement approach to data of 27 subjects. For each subject, the SRLM of the two hemispheres has been segmented in  $\approx 10$  slices resulting in 594 SRLM contours. The algorithm was set to equidistantly sample SRLM thickness at 20 locations along the medial axis. All medial axes and orthogonal lines defining local SRLM thickness were visually verified. Local thickness was correctly represented in  $> 95\%$  of the orthogonal lines. Figure 3 shows typical examples for successful and failed representations, and illustrates the shape variety of the SRLM. In (a – c), common shape variants and their reasonable measurements are displayed. The contours in (d – f) represent increasing deviations from the typical SRLM shape leading to incorrect thickness measurements (thick lines). It can be seen that these errors occur mostly at sites of high bending or where one part of the contour bends significantly different than the opposite part. The branchings seen in (g – h) result from uncertainty during segmentation which is due to similar signal intensities of blood vessels or surrounding structures. Although a reasonable medial axis can be computed, thickness measurements are disturbed by the second branch and it remains unclear which branch represents the SRLM. Instead of neglecting individual thickness measurements, we completely removed cases similar to (d – h) from our analysis (22% of the contours were removed).

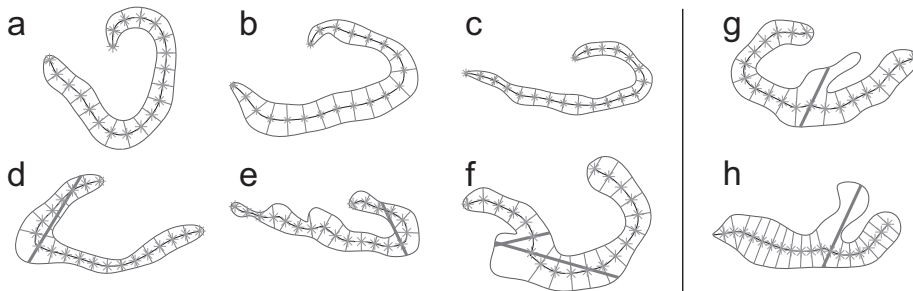


**Fig. 3.** Successful (a-c) and failed (d-h) evaluations of SRLM thickness. Thick lines represent unreasonable measurements due to strong local differences in the bending of the lower and upper SRLM contour parts (d-f) or due to a branching contour (g-h).

The SRLM thicknesses of all subjects had a mean of 0.95 mm ( $\sigma = 0.17$  mm) and showed a very high correlation between both hemispheres ( $r = 0.93, p < 0.01$ ), which suggests that an individual property of the subjects was indeed obtained. Kerchner et al. reported thickness values in the range 0.4 – 0.6 mm [4]. The differences to our values are most likely due to their conservative estimate of where SRLM ends and where surrounding structures begin based on the signal intensities. While they choose the approximate middle of the unsure transition zone, we include the entire zone during segmentation.

## 4 Discussion

Our method is largely dependent on the individual rater bias during pixel-wise delineation of the SRLM. However, if either a conservative or a slightly relaxed segmentation strategy is consistently chosen for all subjects of a study, the bias should be minimized. Hence, comparing a group of subjects with mild Alzheimer disease or Mild Cognitive Impairment and a control group is feasible. We aim at correlating thickness and performance measures of recognition memory tests. Hereby, differences in thickness between groups and reproducible measurements are rather important than absolute real thickness values.

The causes of erroneous thickness measurements as illustrated in Figure 3 (*d–f*), have been also acknowledged by Herron et al. in measuring the corpus callosum (cc) [5]. However, their proposed solution involves a strict anatomically based definition of the cc’s center. The computation of a similar center for the SRLM is hampered by its higher shape variability (Figure 3). A promising solution in regions of high SRLM bending is based on electric field lines and was presented for measuring the cerebral cortex in 2D histological sections [11].

## References

1. Milner B. The Medial Temporal-Lobe Amnesic Syndrome. *Psychiatr Clin North Am.* 2015;28(3):599–611.
2. Thal DR, Holzer M, Rüb U, Waldmann G, Günzel S, Zedlick D, et al. Alzheimer-Related  $\tau$ -Pathology in the Perforant Path Target Zone and in the Hippocampal Stratum Oriens and Radiatum Correlates with Onset and Degree of Dementia. *Experimental Neurology.* 2000;163(1):98–110.
3. Kerchner GA, Hess CP, Hammond-Rosenbluth KE, Xu D, Rabinovici GD, Kelley DA, et al. Hippocampal CA1 Apical Neuropil Atrophy in Mild Alzheimer Disease Visualized with 7-T MRI. *Neurology.* 2010;75(15):1381–1387.
4. Kerchner GA, Deutsch GK, Zeineh M, Dougherty RF, Saranathan M, Rutt BK. Hippocampal CA1 Apical Neuropil Atrophy and Memory Performance in Alzheimer’s Disease. *NeuroImage.* 2012;63(1):194–202.
5. Herron TJ, Kang X, Woods DL. Automated Measurement of the Human Corpus Callosum Using MRI. *Frontiers in Neuroinformatics.* 2012;6(25):1–15.
6. Mueller SG, Stables L, Du AT, Schuff N, Truran D, Cashdollar N, et al. Measurement of Hippocampal Subfields and Age-Related Changes with High Resolution MRI at 4T. *Neurobiology of Aging.* 2007;28(5):719 – 726.
7. Wisse LEM, Gerritsen L, Zwanenburg JJM, Kuijf HJ, Luijten PR, Biessels GJ, et al. Subfields of the Hippocampal Formation at 7T MRI: In Vivo Volumetric Assessment. *NeuroImage.* 2012;61(4):1043 – 1049.
8. Foskey M, Lin MC, Manocha D. Efficient Computation of a Simplified Medial Axis. In: *ACM Symposium on Solid Modeling and Applications*; 2003. p. 96–107.
9. Vollmer J, Mencl R, Müller H. Improved Laplacian Smoothing of Noisy Surface Meshes. *Computer Graphics Forum.* 1999;18(3):131–138.
10. Brandt JW, Algazi VR. Continuous Skeleton Computation by Voronoi Diagram. *CVGIP: Image Understanding.* 1992;55(3):329–338.
11. Schmitt O, Böhme M. A Robust Transcortical Profile Scanner for Generating 2-D Traverses in Histological Sections of Richly Curved Cortical Courses. *NeuroImage.* 2002;16(4):1103 – 1119.